The Double Eyewall and Cycloid-like Track in the Typhoon Dujuan (2003)

Pao-Liang Chang and Jing-Shan Hong

Central Weather Bureau, Taipei, Taiwan, ROC

Abstract

This paper is to document the prominent double eyewall of typhoon Dujuan (2003) in radar view over south of Taiwan. As Dujuan approaching Taiwan, the eyewall radius associated with the outer ring was continuously contracted from about 120 km to 45 km, however, the inner eye was rather inactive and the associated eyewall radius was about 15~20 km and almost kept constant. The intense convection in outer ring was rapidly cyclonic stretched and resulted in a banded structure with thin strip wrapped around the vortex.

The double eyewall in Dujuan was not concentric. Thus the inner eye tended to circulate the outer ring by the steering of the rotational flow in the moat with period of 3.5~4-h and eventually exhibited as a cycloid-like track. The orbited inner eye also contributed to the oscillation of motion speed of the inner eye and the observed maximum inbound/outbound radial velocity. The impact of the oscillated maximum inbound/outbound radial velocity appeared in two folds. First, it produced a wind burst up to 15 m s^{-1} on the inbound/outbound velocity in certain condition depending on the position of the inner eye relative to the typhoon motion. It is very important for the local forecasting or nowcasting of the strong wind. Second, the oscillation of the inbound/outbound velocity associated with the inner eye can enhance the wind shear across the moat. The large differences could enhance the differential rotation in the moat region and result in the inactive inner eye and the spiral band wrapped around the outer ring.

1. Introduction

Intense, highly symmetric tropical cyclones often exhibit concentric eyewall (double eyewall) patterns in radar reflectivity view (Willoughby et al. 1982). The classical concentric eyewall has the deep convection within the inner eyewall surrounded by a nearly echo-free moat, which in turn is surrounded by an outer ring of deep convection. Both convective regions typically contain well-defined tangential wind maxima. The inner wind maximum has the characteristics of large vorticity just inside the radius of maximum wind (RMW), while the secondary wind maximum is usually associated with relatively enhanced vorticity embedded in the outer ring. In contrast, the moat is a region of low vorticity.

The trochoidal motions are often found in double eyewall cases in typhoons or hurricanes. Jordan (1966) marked two cycles' trochoidal motion with the period of about 8-10 hours and the amplitude 23 km in hurricane Calra (1961). Muramatsu (1986) found remarkable oscillations with the period of 5~8-hr and maximum amplitude of 23-km for 36 hrs by land-based radar in typhoon Wynne (1980). Muramatsu (1986) also pointed out that, for some reason, the trochoidal motion occurred when the typhoon eye was displaced at some distance from the system center of the whole typhoon circulation and rotated counterclockwise within storm circulation.

This paper is to document the prominent double eyewall case in the typhoon Dujuan (2003) in radar view when passing over south of Taiwan. Base reflectivity, radial velocity and the derived products were depicted to detail the structure of the double eyewall. Section 2 summarizes the data use and the analysis of the double eyewall, cycloid-like track, and the associated kinematic features are given in section 3.

2. Data and analysis

Digital dataset from Gematronik 1500S Doppler radar located at Kenting (RCKT) were used in this paper. The wavelength and beamwidth of Gematronik 1500S Doppler radar is 10 cm (S-band) and 1°, respectively. Two scan modes in the Gematronik Doppler

radar were adopted to fit the scanning strategy (volume coverage pattern 21, VCP 21) in the WSR-88D Doppler radar. The first mode is for surveillance, which uses low pulse repetition frequency (PRF) to obtain long unambiguous range (460 km) in the lowest two tilts. The second mode with 9 scans uses dual PRF (625 s^{-1} and 469 s^{-1}) to obtain large unambiguous velocity (49.5 m s^{-1}, Frush 1991). There is 1-min difference in between the two scan modes as depicted in Fig. 2 and 3f. Thus, each composite radar volume contains two scan modes with 11 plan position indicator (PPI) scans in 9 elevations and is completed in 8 min.

3. Results

Typhoon Dujuan formed in the West Pacific Ocean at 1200 UTC 29 Aug, 2003; the storm then began a northwestward-moving, passed to the south of Taiwan at 1535 UTC 1 Sep, and made a direct hit on Hongkong at about 1200 UTC 2 September. The best track of typhoon Dujuan over north of South China Sea in 1-hr interval is illustrated in Fig. 1. The figure shows that the storm moved to the northwest by west and exhibited as a small oscillation before passing south of Taiwan. As Dujuan neared Taiwan, the storm moved within the range of the RCKT Doppler radar and could be explored the details about the oscillated track pattern from the radar data analysis.

Fig. 2a is the snapshot of the composite radar reflectivity field at 1159 UTC 1 Sep 2003 and showed a distinct double eyewall in the center of typhoon Dujuan. The double eyewall was evident since the inner eye moved into the observation range of RCKT Doppler radar at 0000 UTC 1 Sep, disorganized as the storm passing over Taiwan at 1535 UTC, re-organized again after passing Taiwan, and extended to 0500 UTC 2 Sep before made landfall at Hongkong. The total life-span was at least lasting for 30-hr. There was no eyewall replacement occurred during

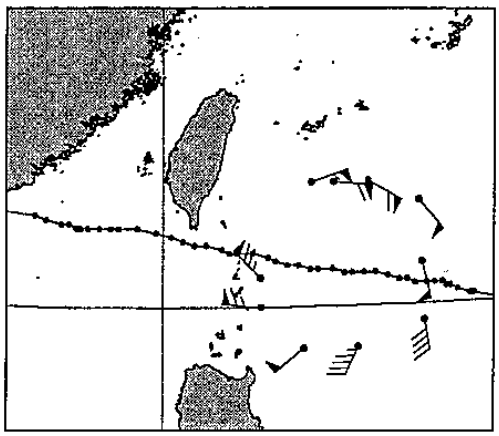

Fig. 1: The track of typhoon Dujuan in 1-h intervals (UTC). The 925-hPa winds (full bar denoted 10 knots) from the dropsonde observations were superimposed.

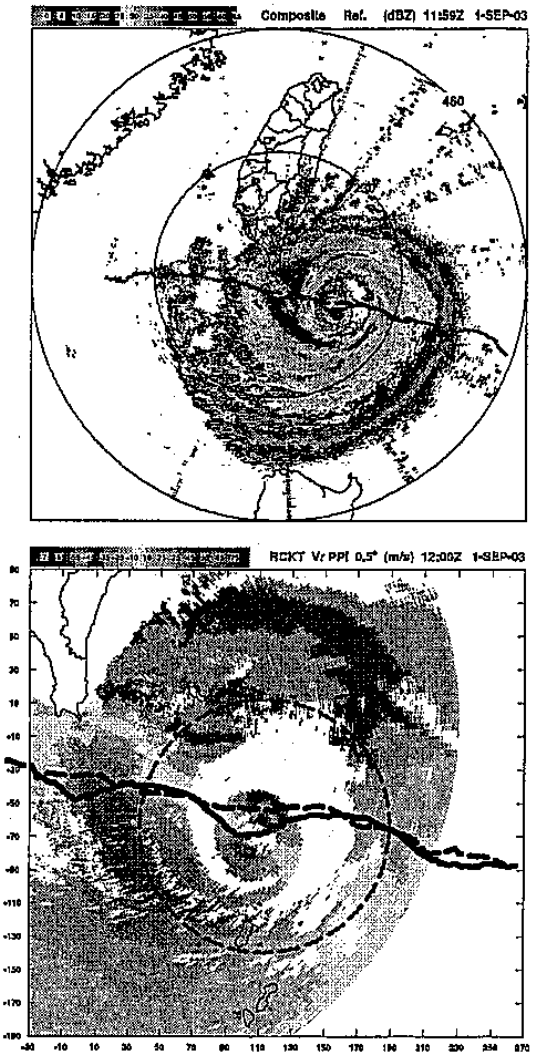

Fig. 2. (a): The snapshot of the composite radar reflectivity field (non-Doppler mode) of 0.5° PPI at 1159 UTC 1 Sep 2003. The track of the outer ring and inner eye derived from the 8-min Doppler radar scans are represented by the dash and solid line, respectively. (b): Doppler velocities of 0.5° PPI at 1200 UTC 01 September 2003. Dash circle is the radius of maximum wind (RMW) calculated by the method of Wood and Brown (1992).

the whole observed lifetime.

As shown in Fig. 2a, the inner eyewall was associated with strong reflectivity up to 55 dBz within radial scale of about 10 km. The outer ring was characterized as broader convective zone around south of Taiwan and the stripped spiral convective bands over east and north of typhoon. The track of the outer ring in 8-min intervals was approximately toward the northwest by west at about 8 m s^{-1} with small fluctuation. The motion of the outer ring was very close to 850-300 hPa deep layer mean wind (8.2 m s^{-1}, 302°) calculated from the composite dropsonde observations that distributed as shown in Fig. 1. This mass-weighted mean wind in Dujuan was about 20 degrees to the right of the storm motion. Similar deviations of the mean storm motion have been documented in a number of studies, e.g. Neumann (1979). Therefore the motion of typhoon Dujuan could be expected to be mostly steered by the environmental flow.

The Doppler velocities (Fig. 2b) exhibited as a dipole Doppler velocity pattern both for the inner and outer eyewall. The maximum inbound/outbound Doppler velocity is 61.0/56.6 and 65.66/62.8 m s^{-1} for the outer and inner eyewall, respectively. The estimated radius of maximum wind (dash ring) for the outer ring is about 76 km. Of particular importance is that the double eyewall in typhoon Dujuan was not concentric. Thus the inner eye tended to circulate due to the steering of the rotational flow in the moat (defined by the echo free area between the inner and outer eyewall). The orbited inner eye superimposed the mean typhoon motion (represented as the motion of the outer ring) therefore resulted in a cycloid-like track pattern of the inner eye. In Dujuan, total of four obviously cycloid-like arches were identified within the range of the radar observations before the typhoon passed over south of Taiwan. Each arch from east to west had the period of 3-h 52-min, 3-h 44-min, 3-h 36-min, and 3-h 20-min, respectively. The period of the arch was slightly decreased as typhoon approaching Taiwan Island.

As Dujuan moved closer to the RCKT, reflectivity field at the 0.5°PPI in 40-min intervals were further analyzed and shown in Fig. 3. Fig. 3 showed that the intense convection in outer ring was rapidly cyclonic stretched and resulted in a banded structure with thin strip wrapped around the vortex. However, the thin strip was mostly wrapped around the outer ring with little interaction with the inner eye. The wrapped strip evolved into more spiral bands and became broader in the following period, which was very similar to the type 1 instability proposed by Kossin et al. (2000) in the hurricane with concentric eyewall. The type 1 instability argued that the central vortex can be dynamically inactive but serves to induce a strong differential rotation in the moat region, which then acts as a barrier to inward mixing of small amplitude asymmetric vorticity disturbances and inhibits to rearrange into a monopole. In the current case we didn't have enough observations to further verify the mechanism of type 1 instability, however, the morphology from the storm evolution was coincident with the description in the Kossin et al. (2002), including the inactive inner eye, the spiral strip wrapped around the outer ring, and the broadening of the outer ring.

Figure 3 showed that the eyewall radius associated with the outer ring was continuously contracted from about 120 km to 45 km (also shown in Fig. 4) while the eyewall radius associated with the inner eye was about 15~20 km and almost kept constant. Fig. 4 exhibited the details of the contraction process and exhibited as two phases, roughly separated from each arch. The first phase was corresponding to arch A and contracted from 120 to 68 km. This period also associated with an obviously spin-up of the tangential wind (estimated as the mean of the maximum inbound and outbound radial velocity) from 48 to 60 m s^{-1} in 2 hours (as shown in Fig. 4). The contraction and spin-up, in particular for the outbound radial velocities, were most significant between 1040~1224 UTC, which was coincident with the active convection occurred over the downstream in between the typhoon and Taiwan topography. Thus, the topography is suggested to enhance the convection over the eyewall range of the outer ring as the storm approaching Taiwan. The deepening of the pressure due to the latent heating supported a sharp tangential wind tendency and eventually resulted in the spin-up and the contraction of the outer ring (Shapiro and Willoughby 1982).

The eyewall radius of the outer ring tended to contract *linearly* from 78 to 45 km in the second phase. However, the tangential

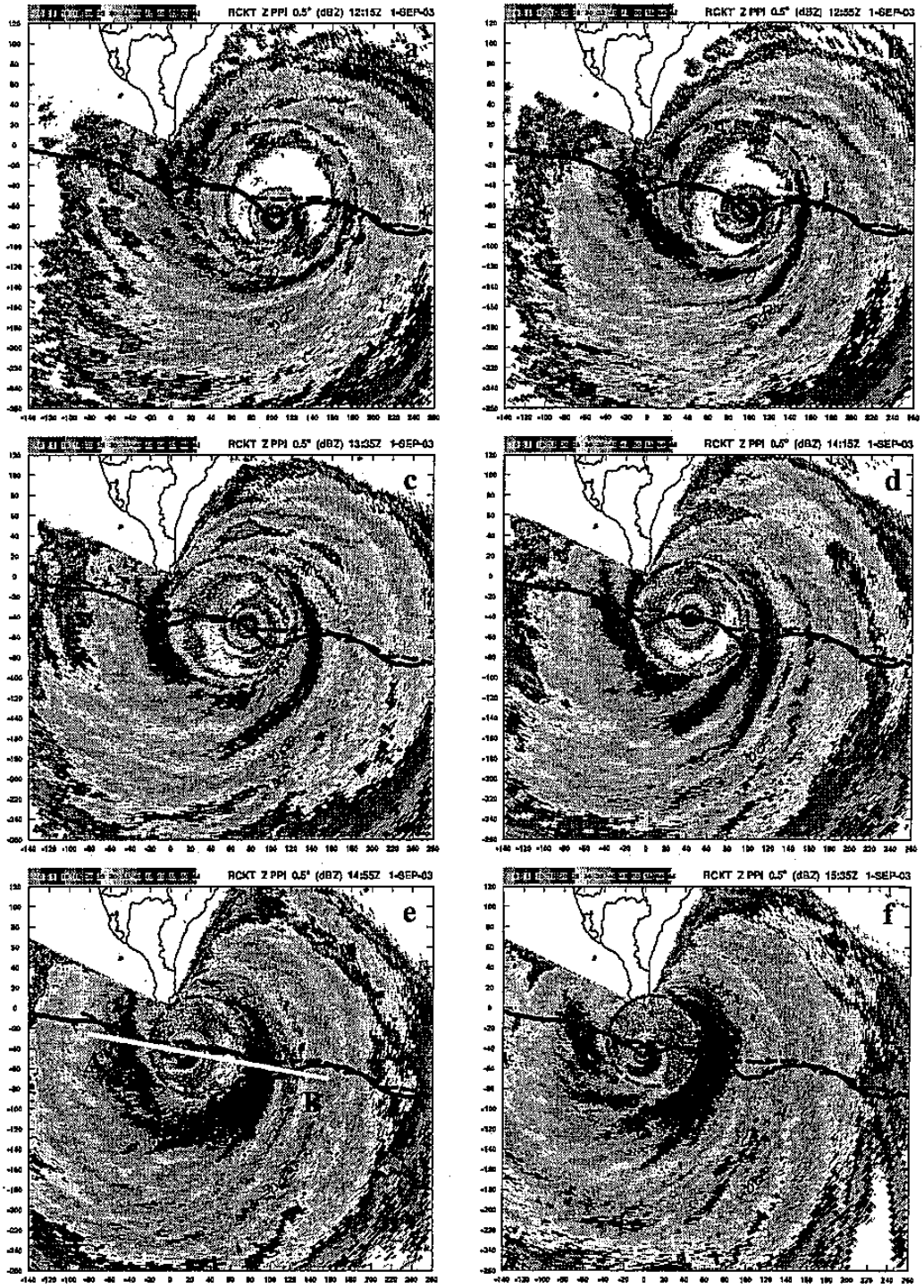

Fig. 3: Same as Fig. 2 but from 0839 to 1159 UTC 1 Sep in 40-min intervals. The circle with dash line is the estimated radius of maximum wind of outer ring.

wind almost kept constant in the beginning of the phase and then spin-down abruptly (especially for the out bound radial velocity) at 1432 UTC. Topography again is suggested to play the role to directly spin down the tangential wind around the outer ring as the storm neared Taiwan further and then increase the inward flow component due to the unbalanced pressure gradient force. This increased inward flow further resulted in the contraction of the outer ring and the enhanced con

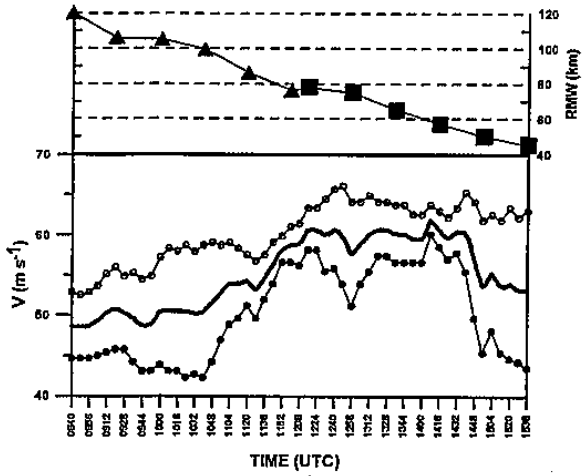

Fig. 4. Time series plot of RMW (above) from 0840 to 1536 UTC, the triangles and squares are corresponding to the RMW in arch A and B, respectively. Belows are the maximum inbound (hollow circles) and outbound (solid circles) radial velocities of the outer ring. The heavy line is the mean of the maximum inbound and outbound velocity.

vection.

As pointed out in Fig. 3, the double eyewall in Dujuan was not concentric. Therefore the inner eye tended to circuit due to the steering of the rotational flow in the moat. The orbiting inner eye resulted in not only the cycloid-like track pattern but also some important kinematic features. For the convenient, we assume typhoon moved toward the west and the radar locates infinity at west as shown in Fig. 5.

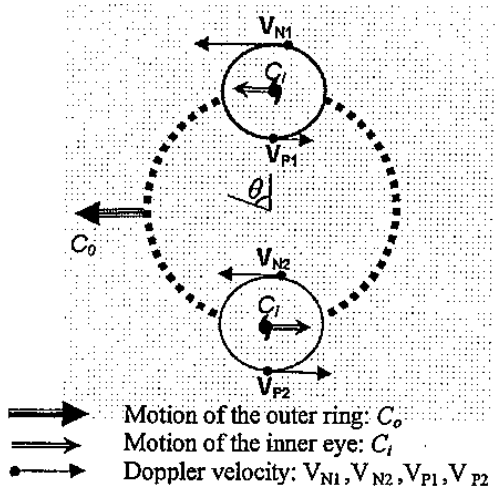

Fig. 5. Schematic diagram of the circular orbit (dashed line) of the inner eye in the moat region and the related kinematic parameters. θ is the azimuthal angle of the orbiting inner eye. The positive (negative) values of Doppler velocity V_N (V_P) indicate outward (inward) the Doppler radar assumed to be located infinity at the west.

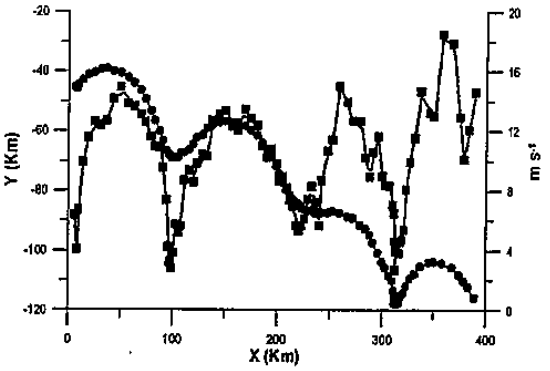

Fig. 6. The position plot (black dots) of the inner eye from 0255 to 1455 UTC 1 Sep. relative to the RCKT Doppler radar. The location of the Doppler radar is at (0, 0). The speed (m s^{-1}) of the inner eye motion was indicated as the square.

Note that the motion speed of the inner eye (C) composed two components: the motion of the outer ring (C_o) and the orbit speed of the inner eye (C_i). C_o could be estimated from the radar observations, while C_i was difficult to be obtained intuitively from the observations. Since the inner eye was orbiting, the motion speed of the inner eye would oscillate and could be expressed as $-C_o-C_i\cos\theta$, where θ is the azimuthal angle. As a result, the maximum (C_{max}) and minimum (C_{min}) speed of the inner eye motion would occur as the inner eye orbited to the north and south, which was at the direction (opposite direction) of the motion of the outer ring; where $C_{max}=|-C_o-C_i|$ and $C_{min}=|-C_o+C_i|$. Since assume typhoon was straightforward to the west, the top (cusp) of the cycloid-like track happened to occur as the inner eye orbited to the north (south), too. Therefore, the maximum (minimum) motion speed of the inner eye would well match as the inner eye moved to the top (cusp) of the arch. The mechanism could explain the oscillated speed of the inner eye motion, which was deviated from about 4 to 14 m s^{-1} and resulted in the correlation coefficient up to 0.92 in between the track pattern and the orbit speed as shown in Fig. 6. Substituting C_{max}~14 m s^{-1} and C_{min}~4 m s^{-1}, the orbit speed of the inner eye (C_i) thus could be estimated by $|(C_{max}-C_{min})/2|$ and given about 5 m s^{-1}. While C_o was about 8 m s^{-1} directly estimated from the radar observations.

To further compare the track of the outer ring and inner eye, one can find the orbit of the inner eye obviously deflect to the south portion of the moat. Fig. 7 depicted the orbit of the inner eye relative to the center of the outer ring for two complete cycloid-like arches sampled from

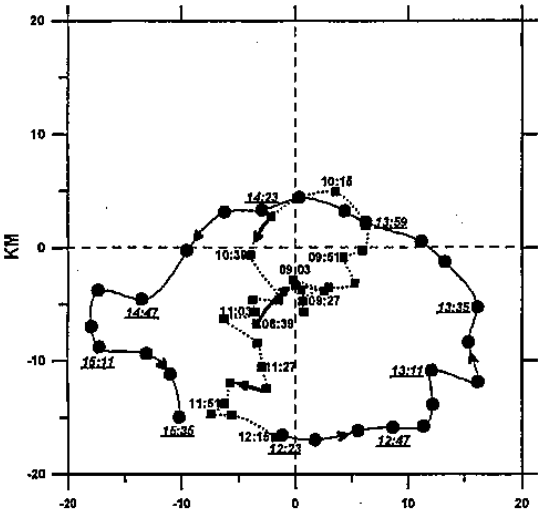

Fig. 7. The orbit of the centers of the inner eye relative to the outer ring. The center of the outer ring is fixed at coordinate of (0, 0). Dashed and Solid lines indicate the orbit of the inner eye in the arches displayed in Fig. 3 and 4, respectively. The numbers in arial and *Italics* are the time stamp in every 24 min for the two arches. The arrays indicate the direction of the orbit.

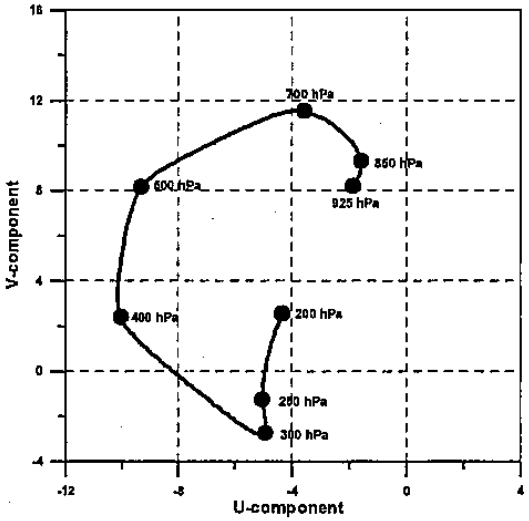

Fig. 8. The hodograph of the environmental wind field derived from the composite dropsonde data.

0839~1215 UTC and 1215~1535 UTC 1 Sep. The periods for the two arches were 3-h 36-min and 3-h 20-min, respectively. The figure showed that the cyclonic oscillation with amplitude about 10-km in the first arch started from 0839 UTC and tended to be rather symmetric to the center of the outer ring. The inner eyes then moved to further south during the end of the arch and started to the beginning of the second arch. The small amplitude and southward moving during the end of the first arch was partially due to the outer ring co-oscillated with the inner eye and resulted in a small oscillated track pattern as depicted in the Fig. 3. However, the amplitude of the second arch was larger than the first one and up to 30 km in the east-west and 20 km in the south-north. The orbit of the inner eye was roughly symmetry in the east-west and obviously shifted to the south portion. The accuracy of the algorithm to determine the centers, in particular for the outer ring, of cause, has its limitations (the uncertainty in general with variations less than 5-km), however, the shift of the orbit of the inner eye to the south of the outer ring in the second arch was remarkable enough beyond the possible uncertainty due to the center determination algorithm described in the section 2. Fig. 8 was the hodograph of the vertical wind shear derived from the composite dropsonde as shown in Fig. 2. The figure displayed a significant northerly vertical shear from 700 to 300 hPa. On the other hand, the vertical development of the inner eyewall was up to 10~12 km whereas only 7 km for the outer ring (Fig. 9). Thus, the inner eye was suggested to experience more forcing of the vertical wind shear than the outer ring and tended to drift to the south portion of the moat.

The Orbited inner eye also contributed to the oscillation of the observed maximum inbound/outbound velocity. Especially, at specific levels where the motion both in storm and inner eyewall are close to mean flow across storm (V_M),

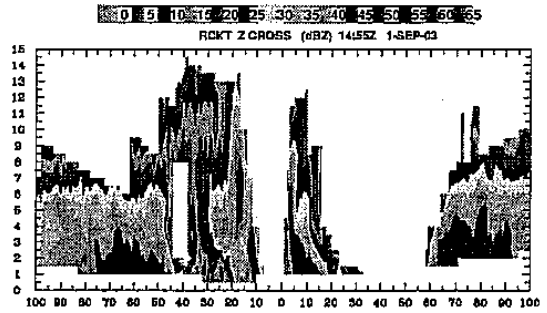

Fig. 9. AB cross-section of the reflectivity field as shown in Fig. 3e.

the mean flow (V_m) across inner eyewall. If only the axisymmertric tangential part of inner eyewall circulation to be considered. The observed inbound/outbound velocities consisted of three components: V_M, V_m, V_T associated with the inner eye. In general, V_T was dominant rather than V_M and V_m. As the inner eye circulated, the maximum inbound (V_N) and minimum outbound (V_P) velocity would occur as the inner eye moved to the north at point N_1 and P_1, while approximate

V_N and V_P would be observed as the inner eye moved to south at point N_2 and P_2. As a result, the Doppler velocity of V_N and V_P would exhibit as an oscillated pattern and be out of phase as shown in Fig. 10.

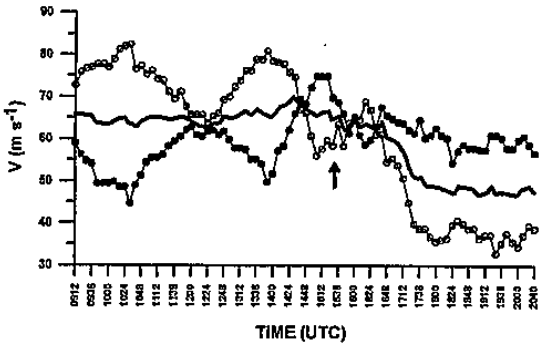

Fig. 10. Time series plot of the maximum inbound (hollow circles), outbound (solid circles) radial velocities, and the mean of the maximum Inbound and outbound radial velocity of the inner eyewall from 0944 to 2138 UTC.The array indicates the time typhoon Dujuan passed over RCKT radar center.

Apparently, the projection of the mo tion of the outer ring and the orbited inner eye to the radial component resulted in the oscillation of the observed inbound and outbound radial velocity. The impact of the oscillation appeared in two folds. First, the projection of V_M and V_m could produce a periodic wind burst up to 15 m s^{-1} in 1~2 hour on the inbound/outbound velocity in certain condition depending on the relative relation of typhoon motion and the orbit of the inner eye. Wakimoto and Black (1994) and Willoughby and Black (1996) studied the Hurricane Andrew and suggested that enhanced swirling motion associated with eyewall mesovortices may cause the intense wind damage at ground level. Nonetheless, the mechian in Dujuan inner eywall is different from mesovortices, but it produced the strong wind that was similar to them and very important for the local forecasting/nowcasting, in particular in the landfall case. Second, the oscillation of the inbound/outbound velocity associated with the inner eye can enhance the wind shear across the moat. For example, the difference of the inbound velocity between the inner eye and outer ring was up to 24 m s^{-1} at 1032 UTC. The large differences could enhance the differential rotation in the moat region and result in the inactive inner eye and the spiral band wrapped around the outer ring, which was very similar to the characteristics of the eyewall structure as the type 1 instability proposed by Kossin et al. (2002).

Acknowledgment

The authors extend the sincere gratitude to the Central Weather Bureau of Taiwan for offering the utmost support. This research was supported by the National Science Council of Taiwan under Grant NSC 92- 2119-M-052-002-AP1 and NSC 92-2111-M- 052-002-AP2.

Reference

Frush, C. L., 1991: A graphical representation of the radar velocity dealiasing problem. Preprints, *25th Int. Conf. on Radar Meteorology*, Paris, France, Amer. Meteor. Soc., 885 - 888.

Jordan, C. L., 1966: Surface pressure variations at coastal stations during the period of irregular motion of Hurricane Carla of 1961. *Mon. Wea. Rev.*, **94**, 454 – 458.

Kossin, J. P., Schubert, W. H., Montgomery, M. T., 2000: Unstable Interactions between a Hurricane's Primary Eyewall and a Secondary Ring of Enhanced Vorticity. *J. Atmos. Sci.*, **57**, 3893 – 3917.

Muramatsu, T., 1986: Trochoidal motion of the eye of Typhoon 8019. *J. Meteor. Soc. Japan*, 64, 259-272.

Neumann, C. J., 1979: On the use of deep-layer-mean geopotential height fields in statistical prediction of tropical cyclone motion. *Sixth Conference on Probability and Statistics in Atmospheric Sciences*, Banff, Alberta, AMS, 32-38.

Shapiro, L. J., and H. E. Willoughby, 1982: The response of balanced hurricanes to local sources of heat and momentum. *J. Atmos. Sci.*, **39**, 378–394.

Wakimoto, R. M., and P. G Black, 1994: Damage survey of Hurricane Andrew and its relationship to the eyewall. *Bull. Amer. Meteor. Soc.*, **75**, 189-200.

Willoughby, H.E., J. A. Clos, and M. G. Shoreibah, 1982: Concentric eye walls, secondary wind maxima, and the evolution of the hurricane vortex. *J. Atmos. Sci.*, **39**, 395–411.